# Pattern formation by boundary forcing in convectively unstable, oscillatory media with and without differential transport

Patrick N. McGraw and Michael Menzinger
*Department of Chemisty, University of Toronto, Toronto, Ontario, Canada M5S 3H6*
(Received 17 December 2004; published 17 August 2005)

Convectively unstable, open reactive flows of oscillatory media, whose phase is fixed or periodically modulated at the inflow boundary, are known to result in stationary and traveling waves, respectively. The latter are implicated in biological segmentation. The boundary-controlled pattern selection by this flow-distributed oscillator (FDO) mechanism has been generalized to include differential flow (DIFI) and differential diffusion (Turing) modes. Our present goal is to clarify the relationships among these mechanisms in the general case where there is differential flow as well as differential diffusion. To do so we analyze the dispersion relation for linear perturbations in the presence of periodic boundary forcing, and show how the solutions are affected by differential transport. We find that the DIFI and FDO modes are closely related and lie in the same frequency range, while the Turing mechanism gives rise to a distinct set of unstable modes in a separate frequency range. Finally, we substantiate the linear analysis by nonlinear simulations and touch upon the issue of competition of spatial modes.

DOI: 10.1103/PhysRevE.72.026210 PACS number(s): 82.40.Bj, 82.40.Ck, 47.70.Fw

## I. INTRODUCTION

Recently, theoretical [1–15] and experimental [5,16–22] attention has been focused on spatiotemporal instabilities in one-dimensional reactive flows. Among these pattern-forming instabilities are the differential flow instability [9,21,25,10], Turing [23,24], and the physically distinct flow-distributed oscillation (FDO) [1,5,7,19,8] mechanisms. Two of these, DIFI and FDO, necessarily involve a flow, while Turing and DIFI necessarily involve the differential transport of activator and inhibitor species.

In a flowing medium instabilities may be absolute or convective [26–28,2,3]. In the first case, a localized disturbance grows with time and spreads both upstream and downstream. In the convective case, on the other hand, a localized disturbance cannot propagate upstream, and so the effect of a temporary, local perturbation is eventually washed downstream and out of the system. However, persistent disturbances upstream can have a large effect on the downstream behavior. This leads to the possibilities of patterns which are controlled primarily by the *upstream* boundary conditions and of noise-sustained structures [28,27]. We are interested here in the convective case, where the upstream boundary is crucial to the control of the pattern. FDO is a convective mechanism of pattern formation whereby an open flow maps the temporal dynamics of an oscillating medium, whose phase is set at the upstream boundary, onto space.

A fixed boundary condition results in stationary waves [2,1,5,19,3,4], while time-periodic boundary conditions give rise to upstream and downstream traveling [5,18,19] and pulsating [18,19] waves with periodicity equal to that of the boundary. In the kinematic limit of fast flow and/or vanishing diffusion these waves arise from the phase dynamics of the oscillating medium [5,7,8,19]. Analytic expressions for the phase velocity $c$ and wavelength $\lambda$ of the phase waves in this limit are given in Refs. [7,8,19]. The phase dynamics makes FDO conceptually the simplest of the pattern-forming mechanisms, although it was discovered later than the others. When diffusion becomes important (at a sufficiently low flow rate) and the system comes close to the reaction-diffusion limit, the structures may be damped or their wave forms may be modified significantly from the dynamics of the local system [14]. The Turing instability, by contrast, was initially conceived of as an absolute instability of a stationary reaction-diffusion medium. In a flow system, however, Turing [8,22,20], DIFI [13], bistable [8] patterns, and even structures in passive media [8] can also be generated and controlled convectively by the upstream boundary condition.

Since an open flow with a fixed upstream boundary is equivalent, via a Galilean transformation, to a stationary medium with a moving boundary [6–8,20], the physical ideas of FDO and other boundary-driven convective instabilities are also applicable to growing media. In developmental biology a FDO mechanism driven by an oscillator or "segmentation clock" at the growth tip of an embryo leads to the formation of somites, the precursors of vertebrae and body segments during early embryogenesis [6–8,20] (the best-studied examples are chick and mouse). Quite generally, pattern formation on a growing domain is vitally important in developmental biology [29,30]. Recent experiments [20,22,32] in Turing and in Hopf unstable media also make use of a moving boundary that is equivalent to a flow. By contrast, the packed bed reactor (PBR) is a flow reactor in which the inlet, not the medium, is fixed in the laboratory frame of reference. In the experiments of [5,18,19,16,17] the reactor is fed by the outlet of a continuous stirred tank reactor (CSTR) which can be made to oscillate, generating traveling waves in the PBR tube, or remain at a fixed point, leading to stationary waves.

Satnoianu *et al.* [11,12] generalized the FDO scenario by allowing differential transport (different flow rates and/or diffusion rates) to act on the key chemical species. They suggested that the resulting waves be viewed as variants of a general mechanism called flow- and diffusion-distributed

 

structures (FDS). In Ref. [12], traveling waves and combinations of differential flow and diffusion were also considered. Traveling waves were referred to as DIFI while stationary waves were referred to as FDS.

The goal of the present work is to understand what contribution differential transport makes to the basic FDO scenario and to clarify the relationships among the convectively driven FDO and the differential transport (Turing and DIFI) modes in an open flow. We develop a general linear stability analysis for convective modes driven by boundary perturbations and illustrate the results by plotting solutions of the dispersion relations. Our approach differs from that of Refs. [11–13] in several ways. First, we choose to focus on patterns driven convectively by the upstream boundary condition, to distinguish them from absolute instabilities. We do this because the possibility of convective instability embodies much of the additional behavior that is possible with a flow (or growth) as opposed to a stationary medium. Accordingly, we treat the dispersion relation for small disturbances differently, taking the real frequency, set by the boundary condition, as the independent variable and examining the *spatial* behavior of the resulting disturbance rather than examining the temporal behavior of an imposed spatial perturbation. We consider a mode unstable if it grows with downstream *distance* in response to a constant or periodic driving at the boundary. This approach resembles that of Refs. [1,14] and was also considered in Ref. [26] in the context of plasma physics.

Within this approach we find it unnecessary to distinguish sharply between stationary and traveling modes as was done in Ref. [13]; all are treated within the same dispersion relation, and stationary modes simply correspond to the particular case of zero frequency. We find instead that an examination of the dispersion relation results in a natural grouping of the modes showing that the FDO and DIFI mechanisms are closely related to each other, both being associated with an underlying Hopf instability, while the Turing mechanism gives rise to a distinct set of modes. The two sets of modes show up as separate peaks in different frequency ranges, and are also clearly distinguished by other criteria including the phase velocity and the relative phase between oscillations of the activator and inhibitor. The DIFI and FDO modes can be either traveling or stationary, while Turing modes are stationary only in the case of zero flow. In that case (the case in which the Turing mechanism was originally considered), the instability is absolute and therefore not controlled by the boundary. However, it has been observed that Turing patterns can be generated by boundary forcing in a system with nonzero flow [8,20,22] in which case they are advected by the flow, i.e., they are stationary in the comoving frame. In this case the instability can be convective and a Turing mode with a particular wavelength can be selected by imposing a periodic perturbation at the inflow. We find that in the presence of simultaneous differential flow and differential diffusion (relevant to the packed bed reactor) some of the distinguishing features of Turing modes are modified, but the essential picture of two separate peaks remains unchanged.

At the end of the paper, we illustrate the results of our linear analysis by some nonlinear simulations. We find that the linear results give a rather good insight into the nature of the fully nonlinear solutions, at least in the case where the nonlinearity is not very strong. Finally we observe and comment on the competition of wave modes.

## II. LINEAR ANALYSIS OF RDA EQUATIONS

We consider the reaction-diffusion-advection (RDA) equations describing the chemical kinetics and transport of an activator and an inhibitor species. The chemical medium is defined by the "local" or batch reactor dynamics together with transport terms. We wish to consider several forms of differential transport, so we allow each species to have its own flow velocity and diffusion coefficient. The RDA equations are

$$\frac{\partial A}{\partial t} = f(A,B) - \phi_A \frac{\partial A}{\partial x} + D_A \frac{\partial^2 A}{\partial x^2},$$

$$\frac{\partial B}{\partial t} = g(A,B) - \phi_B \frac{\partial B}{\partial x} + D_B \frac{\partial^2 B}{\partial x^2}. \tag{1}$$

Our aim is to analyze the pattern-forming instabilities, so we shall assume that the local kinetics has a stable or unstable fixed point, and linearize the equations for small perturbations of the uniform fixed point state. For convenience, we shall use units in which the flow velocity of species $B$ is unity. Linearizing near the fixed point $(A_0, B_0)$, transforming the units to ones where $\phi_B = 1$, and defining the velocity and diffusion ratios $\delta_v = \phi_A / \phi_B$ and $\delta_D = D_A / D_B$, respectively, and $D = D_B$ gives

$$\frac{\partial a}{\partial t} = -\delta_v \frac{\partial a}{\partial x} + \delta_D D \frac{\partial^2 a}{\partial x^2} + a_{11} a + a_{12} b,$$

$$\frac{\partial b}{\partial t} = -\frac{\partial b}{\partial x} + D \frac{\partial^2 b}{\partial x^2} + a_{21} a + a_{22} b, \tag{2}$$

where the matrix

$$\frac{\partial(f,g)}{\partial(a,b)} = \begin{pmatrix} a_{11} & a_{12} \\ a_{21} & a_{22} \end{pmatrix}$$

is the Jacobian of the local kinetic system evaluated at the fixed point and $a = A - A_0$, $b = B - B_0$ are the perturbations. A complex exponential solution

$$\begin{pmatrix} a \\ b \end{pmatrix} = \begin{pmatrix} u \\ v \end{pmatrix} e^{iwt + kx} \tag{3}$$

represents a traveling wave in which the concentrations of both species oscillate.[1] The relative amplitude and phase are determined by the complex amplitudes $u$ and $v$. [A real solution is formed from Eq. (3) and its complex conjugate.] Substitution into Eq. (2) gives

$$i\omega u = -\delta_v k u + \delta_D D k^2 u + a_{11} u + a_{12} v,$$

[1]The phase convention of the wave number $k$ is that of Ref. [12], chosen for later convenience. Re $k$ represents the spatial growth rate, while $-\mathrm{Im}\, k$ is the inverse wavelength or "real" wave number.

$$i\omega v = -kv + Dk^2 v + a_{21}u + a_{22}v, \tag{4}$$

which can be combined to give the dispersion relation

$$\begin{aligned} 0 &= \delta_D D^2 k^4 - (\delta_D + \delta_V) D k^3 \\ &+ D[a_{11} + \delta_D a_{22} + \delta_V/D - i\omega(\delta_D + \delta_V)]k^2 \\ &+ [-(a_{11} + \delta_V a_{22}) + i\omega(1 + \delta_V)]k + \Delta - i\omega \mathrm{Tr} - \omega^2, \end{aligned} \tag{5}$$

where $\mathrm{Tr} = a_{11} + a_{22}$ and $\Delta = a_{11}a_{22} - a_{12}a_{21}$ are, respectively, the trace and determinant of the Jacobian. Two particular cases of differential transport were studied in previous work. The case $\delta_V = 1$, $\delta_D \neq 1$ is relevant to the moving-boundary experiments [22] in which there is differential diffusion due to the immobilization of one of the species, but the flow velocities are the same, since it is actually the boundary that moves relative to the medium. On the other hand, Satnoianu *et al.* [12] considered the case $\delta_V = \delta_D \neq 1$, which may be a good approximation in a PBR-type flow system when one of the species is immobilized and the other moves freely. The pure FDO case $\delta_V = \delta_D = 1$ has no differential transport. With the appropriate changes of variables and restrictions on the transport ratios, the above dispersion relation reduces to the ones given in the previous references [1,8,12–14] for particular cases. We wish to consider more general forms of differential transport, for both theoretical and experimental reasons. First, varying the two transport ratios independently allows a fuller understanding of the effects of the two types of differential transport and their interaction. Second, we wish to allow the possibility of experiments in which the transport coefficients are related in ways other than those previously considered.

We analyze the steady-state response of the system to a sinusoidal forcing of the inflow boundary at a constant amplitude. In general, in the linear approximation, this gives rise to a traveling wave with a complex wave number and a frequency equal to the forcing frequency. The frequency $\omega$ will be taken to be purely real, reflecting the constant amplitude of the forcing. However, the convective dynamics of the medium may cause the disturbance to grow or damp with the downstream distance, so that $k$ may be complex. Thus, we consider the real $\omega$ as an independent variable and solve the dispersion relation numerically for the complex $k$. The dispersion relation is quartic in $k$ and so it has in general four solutions. Each is associated with an eigenvector $\mathbf{u} = \binom{u}{v}$ which can be found by substituting the solution $k$ back into Eq. (4). In this way we can find $k(\omega)$ and $\mathbf{u}(\omega)$. The ratio $R(\omega) \equiv v/u$, which in general is complex and frequency dependent, gives information about the relative amplitude and phase of oscillations in the two species (an example is discussed below). We will see that in general the four solutions comprise two pairs, of which only one pair is relevant to the system's behavior near the upstream boundary. The two solutions of a pair together give one physical oscillation mode with an arbitrary phase.

### A. Pure FDO: $\delta_V = \delta_D = 1$

To illustrate the physical meaning of the dispersion relation, we consider first the simplest case of pure FDO, in which $\delta_V = \delta_D = 1$. It can easily be verified that in this case the dispersion relation (5) does not depend on the Jacobian matrix elements separately, but only on the trace and determinant. The pair of equations (4) can then be diagonalized completely by changing coordinates to the eigenbasis of the Jacobian, and the quartic dispersion relation factorizes into two quadratic ones as derived in Ref. [14], one for each eigenvector. The quadratic dispersion relations depend on the Jacobian eigenvalues, which are given by

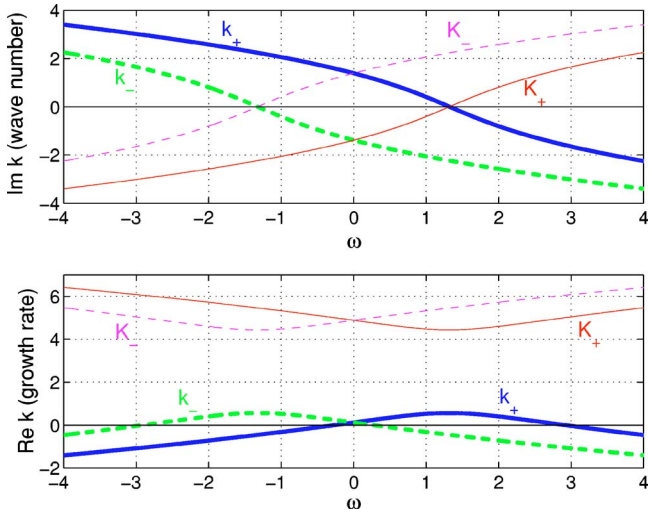


FIG. 1. (Color online) All four solutions of the dispersion relation for the pure FDO case with a Hopf unstable local system and no differential transport. The two lower solutions are labeled $k_\pm$ and the two upper solutions are $K_\pm$. $K_+$ and $k_+$ are both associated with the eigenvector $\mathbf{u}_+$ and the other two with $\mathbf{u}_-$.

$$\lambda_\pm = \mathrm{Tr}/2 \pm \sqrt{\mathrm{Tr}^2/4 - \Delta} \tag{6}$$

and are complex conjugates if $\mathrm{Tr}^2/4 - \Delta < 0$. For the sake of simplicity we consider the particular case with

$$\mathbf{J} = \begin{pmatrix} 1 & 1 \\ -1 & 1 \end{pmatrix}, \tag{7}$$

whose eigenvalues and eigenvectors are $\lambda_\pm = 1 \pm i$ and

$$\mathbf{u}_\pm = \begin{pmatrix} 1 \\ \pm i \end{pmatrix}. \tag{8}$$

In general, the relative amplitude of the two components is complex for an oscillatory system, indicating a phase difference between the two components. In this particular case, the phase difference is $\pi/2$. A plot of the four solutions $k_m(\omega)$ $(m = 1,2,3,4)$ then has the form shown in Fig. 1. There are two solutions associated with each of the two eigenvectors, of which one has a much larger real component. Both solutions are necessary in order to satisfy a boundary value problem in which boundary conditions are specified at $x = 0$ and at some downstream point $x = L$. However, it has been argued [27] that for quite general boundary conditions at a far away downstream boundary, it is the solution with the *less* positive growth rate that predominates near the upstream boundary $(x \ll L)$. As an example, consider

adjusting the coefficients $A$ and $B$ in the general solution $Ae^{\kappa_1 x}+Be^{\kappa_2 x}$ (with $\kappa_2 > \kappa_1$) so as to satisfy either Dirichlet or Neumann boundary conditions at $x=L$. In either of these cases, $B$ is smaller than $A$ by a factor of order $e^{(\kappa_2-\kappa_1)L}$. Therefore, when there is a clear separation between the pairs of solutions, the one with lower growth rate dominates everywhere but close to the downstream boundary, which we take to be far away compared to the growth or damping length scales ($|\kappa_{1,2}|L \gg 1$). The same conclusion can be reached by applying the reasoning of Ref. [26]. In that work it was shown that, in the absence of absolute instabilities, a true spatially amplifying (convectively unstable) mode can be identified as one whose wave number crosses the imaginary axis when a large negative imaginary constant is added to the frequency. In the dispersion relations (4) and (5), adding a negative imaginary constant to the frequency is equivalent to adding a negative constant to the trace of the Jacobian, i.e., adding damping to the internal dynamics. When such damping is added, the two solution branches move apart, so that the upper solutions never cross the axis while the lower solutions may do so. We therefore focus attention on the lower solutions with smaller growth rates. These two solutions are associated with the two eigenvectors of the Jacobian, so we label them $k_\pm$. They are complex conjugate mirror images of each other under reflection through the vertical axis $[k_+(\omega)=k_-^*(-\omega)]$ and represent the same physical wave solution, namely,

$$\begin{pmatrix} a \\ b \end{pmatrix} = \mathrm{Re}(e^{i\omega t}e^{k_+ x}\mathbf{u}_+) = \mathrm{Re}(e^{-i\omega t}e^{k_- x}\mathbf{u}_-)$$

$$= \begin{pmatrix} \cos(\omega t + \mathrm{Im}\, k_+ x) \\ \sin(\omega t + \mathrm{Im}\, k_+ x) \end{pmatrix} e^{(\mathrm{Re}\, k_+)x}. \quad (9)$$

Because of this reflection symmetry, it will be convenient in the remainder of the paper to plot only one solution, with the understanding that the reflected complex conjugate is also present.

Figure 1 shows the growth rates and wave numbers for all four solutions. Note the following. (1) Im $k$ has a zero at the natural frequency $\omega=\omega_0=\sqrt{\Delta-\mathrm{Tr}^2/4}$. When Im $k=0$, the phase velocity

$$c = -\omega/\mathrm{Im}\, k \quad (10)$$

has a corresponding pole, as will be seen in Figs. 2–5. Disturbances at precisely the natural frequency result in growing uniform ($k=0$) oscillations of the medium (this is essentially the batch Hopf mode) while perturbations faster or slower than $\omega_0$ give downstream or upstream traveling waves, respectively, similarly to the kinematic results [5,8]. Stationary waves occur for $\omega=0$. As shown in Ref. [14], the sharpness of the growth rate peak depends on the dimensionless quantity $D\,\mathrm{Tr}/\phi^2$. Increasing the value of $D$ (or, equivalently, reducing the flow velocity) makes the peak sharper and narrower and reduces the gap between the upper ($K_\pm$) and lower ($k_\pm$) solutions, until, at the threshold of absolute instability, the growth rate curve develops a cusp and the upper and lower solutions cross. When the growth rate curves of the two solutions cross, it is no longer correct to view the solution in the bulk as being determined primarily by the upstream boundary condition—it is also strongly influenced by downstream conditions. This is the signature of an absolute rather than a convective instability. The peak of the growth rate occurs precisely at the frequency defined by the imaginary part of the Jacobian eigenvalue. If the fixed point is not Hopf unstable but instead has eigenvalues $\alpha \pm i\beta$ with $\alpha = \mathrm{Tr}/2 \leqslant 0$, then the picture is qualitatively the same, except that the peak remains below the horizontal axis. Thus all perturbations are damped in this case, but the most slowly damped ones are at the natural frequency.

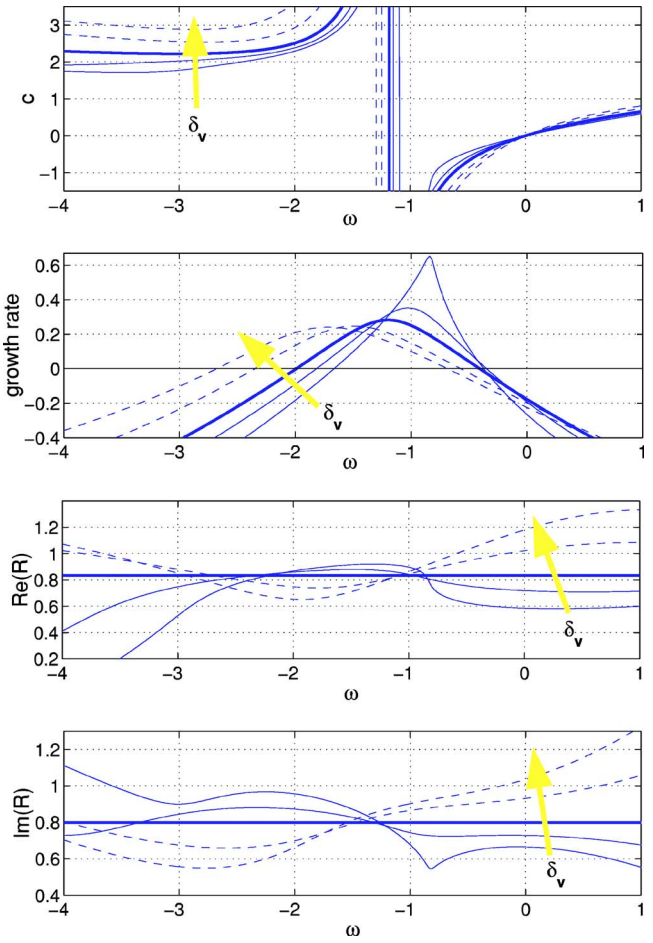


FIG. 2. (Color online) Effect of differential flow on the FDO peak. FN model, $\varepsilon=1.5$, $D=0.1$, $\delta_D=1$. $\delta_v=0.5, 0.75, 1, 1.5, 2$. For the family of curves, the arrows show the direction of increasing $\delta_v$. Dashed lines, $\delta_v>1$; solid thin lines, $\delta_v<1$; thick line, $\delta_v=1$. Note that for the pure FDO case ($\delta_v=1$), the amplitude ratio $R$ is constant, corresponding to an eigenvector of the Jacobian. In the presence of differential transport, however, $R$ becomes frequency dependent. The imaginary part of the amplitude ratio is related to the relative phase of the two components.

The pure FDO case can be viewed as a "baseline" for the physical interpretation of the dispersion relations and their solution curves in the presence of differential transport. Differential transport will modify the shapes of the curves, and will make the eigenvectors $\omega$ dependent and no longer coincident with those of the Jacobian.

Finally, note that in the case when the fixed point is an unstable node rather than a focus, the Jacobian has distinct

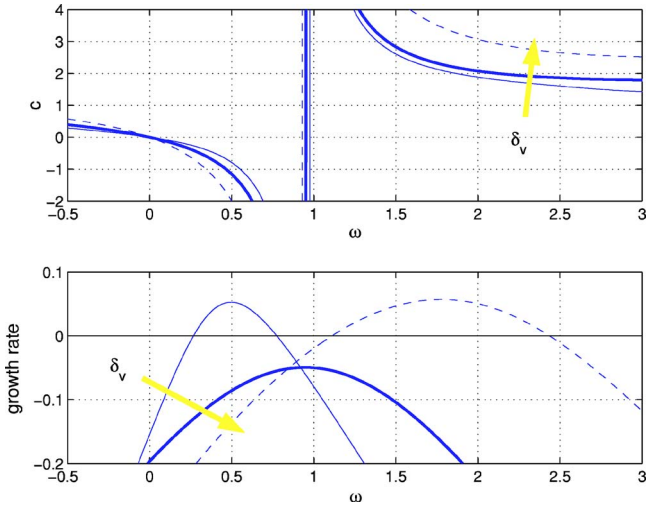


FIG. 3. (Color online) An example of the differential flow instability. FN model, $\varepsilon=0.9$, $D=0.2$, $\delta_D=1$, $\delta_v=0.5$ (thin solid line), 1 (thick line), 2 (dashed line). In the absence of differential flow, there are no unstable modes, but there is nonetheless a peak in the (negative) growth rate at the natural oscillation frequency. Sufficiently strong differential flow shifts the peak so that it rises above zero and unstable traveling wave modes appear. For $\delta_v>1$ (dashed line), the unstable modes are downstream traveling waves; for $\delta_v<1$ (thin solid line) they are upstream. The medium remains stable against uniform oscillations. Viewed in this way, the differential flow instability can be viewed as simply a continuous deformation of the FDO instability.

real eigenvalues and eigenvectors instead of complex conjugate pairs. Peak growth rates for the modes along both eigenvectors then occur at $\omega=0$ [14]. The above results are universal for any system with a Hopf instability.

### B. The effects of differential transport

With the pure FDO case as a comparison, we now examine the effects of differential transport and the convective, boundary driven manifestations of DIFI and Turing instabilities. Typical results are shown in Figs. 2–5 using the Fitzhugh-Nagumo-like [31] (FN) model (11), (12) for the local dynamics.

The key features of the relevant solutions in the FDO case are that $k_+$ has a growth peak and the associated phase velocity has a pole at positive $\omega$, while $k_-$ has a peak and pole on the opposite side, $\omega<0$. A brief summary of the effects of differential transport on the dispersion relation solutions is as follows.

(1) The primary effect of differential flow is to displace and distort the positive-$\omega$ peak of $k_+$ (and its mirror image in $k_-$). Depending on the details of the model, the peak may be shifted to the left, right, upward or downward. The pole in the phase velocity may also be shifted left or right. If sufficiently strong, differential flow can raise the peak growth rate from negative to positive, thus giving an instability even for a stable fixed point. This is precisely what happens in DIFI. For $\delta_V\neq 1$, the peak growth rate may occur quite far from the pole of the phase velocity; thus the strongest instability is to a traveling wave solution rather than to a uniform oscillation.

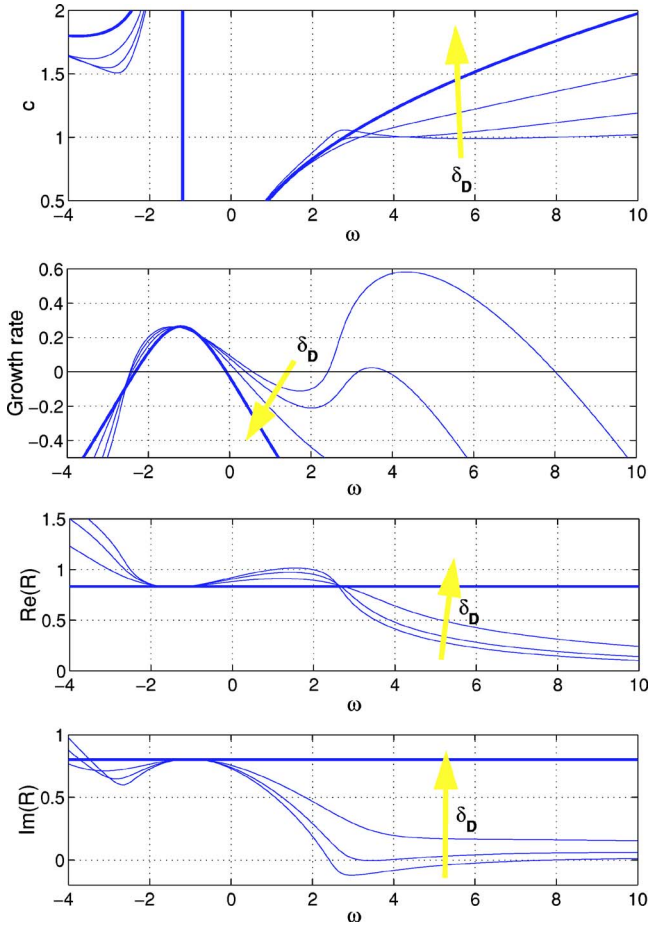


FIG. 4. (Color online) The effect of differential diffusion on the dispersion relation in the absence of differential flow. FN model, $\varepsilon=1.5$, $D=0.2$, $\delta_v=1$. $\delta_D=0.1, 0.25, 0.5, 1$. Thick line, $\delta_D=1$; thin lines, $\delta_D<1$. Arrows show the direction of increasing $\delta_D$. As $\delta_D$ decreases, the FDO peak is distorted slightly, but much more noticeable is the growth of a second peak. The modes in this latter peak can be identified as Turing modes. Their phase velocity is close to 1, and their amplitude ratio is almost purely real. Near the FDO peak, on the other hand, the amplitude ratio is close to that of an eigenvector of the Jacobian.

(2) The most important effect of differential diffusion in the absence of differential flow ($\delta_D\neq 1, \delta_v=1$) is to alter the shape of the negative-$\omega$ tail of the $k_+$ solution (or, equivalently, the positive tail of $k_-$). For fast inhibitor diffusion ($\delta_D<1$) the negative tail can develop first an inflection point and then a second growth rate peak. The modes within this second peak are distinguished by the following features, confirming their interpretation as Turing patterns imposed by the boundary condition and advected with the flow. (A) Their phase velocities are all very close to unity (in units where the flow velocity is 1) showing that they are stationary in the comoving frame. (B) The amplitude ratio $R$ from the associated eigenvector is almost purely real, meaning that, contrary to the situation in self-sustained oscillations, there is no phase lag between the two species (the activator and inhibitor are almost exactly in phase or $\pi$ out of phase).

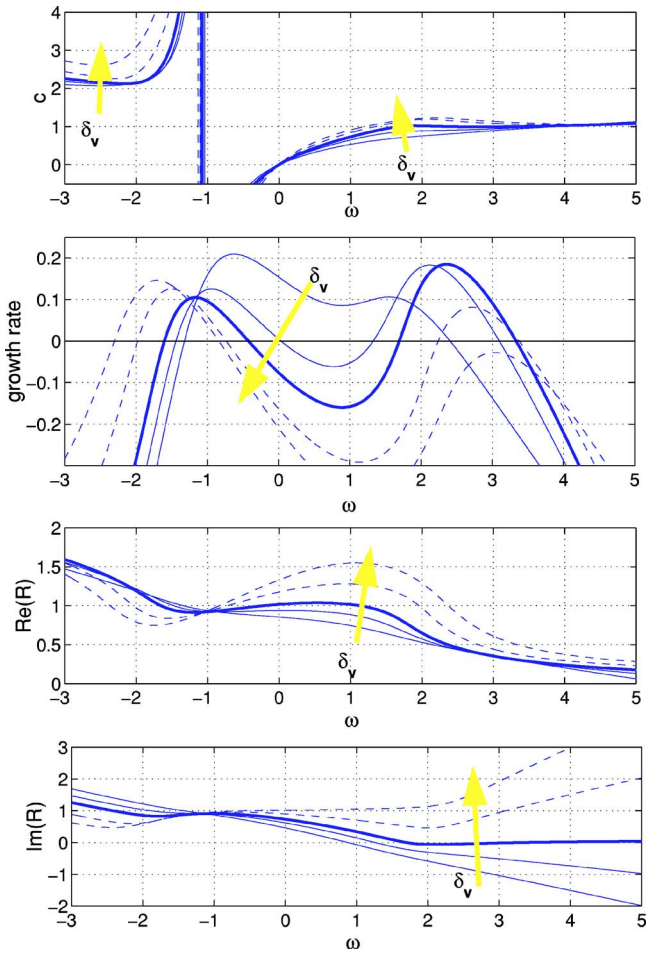


FIG. 5. (Color online) Interacting effects of differential flow and diffusion. Here the differential diffusion is constant, and the velocity ratio is varied. FN model, $\varepsilon=1.2$, $D=0.05$, $\delta_D=0.15$. $\delta_v=0.5,0.75,1,1.5,2$. Thick curve, $\delta_v=1$; thin solid curves, $\delta_v<1$; dashed curves, $\delta_v>1$. With increasing flow ratio, the two peaks are shifted closer together and begin to merge. Departure from equal flow in either direction raises the height of the FDO peak while lowering the Turing peak. Departure from equal flow also causes the phase velocities of the Turing modes to depart from 1.

For the most general case of differential transport, then, the dispersion relation has either one or two peaks, which we can identify as Hopf-FDO-DIFI and Turing peaks, respectively. Changing $\delta_D$ can alter the shape of the FDO peak and conversely, $\delta_V$ can alter the Turing peak, but they generally retain a separate identity, and for the most part exist in a "seesaw" relation.

We now illustrate these statements using examples based on particular models for the form of the Jacobian. The examples we present in Figs. 2–5 and the nonlinear simulations used a form of the FitzHugh-Nagumo model [31], for which the local dynamics is given by

$$\frac{dA}{dt} = \varepsilon(A - A^3 - B),$$

$$\frac{dB}{dt} = -B + 2A, \tag{11}$$

and the Jacobian is

$$\mathbf{J} = \begin{pmatrix} \varepsilon & -\varepsilon \\ 2 & -1 \end{pmatrix} \tag{12}$$

where $\varepsilon$ is a control parameter. [For the linearized analysis, only the Jacobian (12) is needed.] $A$ and $B$ play the roles of activator and inhibitor, respectively. A Hopf bifurcation occurs at $\varepsilon=1$; the fixed point is unstable for $\varepsilon>1$. We also studied another model using the simpler Jacobian

$$\mathbf{J} = \begin{pmatrix} \alpha & 1 \\ -1 & \alpha \end{pmatrix} \tag{13}$$

with control parameter $\alpha$ and Hopf instability for $\alpha>0$, hereafter referred to as the "$\alpha$ model." For the $\alpha$ model with $\alpha>0$, both species are autocatalytic, but one inhibits the other. In most cases, qualitatively similar results were obtained for both models. When the results for the $\alpha$ model differ from those of the FN model, we describe them verbally.

Figure 2 shows typical effects of differential flow on the FDO peak. Differential flow with either fast inhibitor or fast activator transport shifts the position and height of the peak growth rate. It can also shift slightly the location of the pole in the phase velocity (i.e., the zero of Im $k$) but usually this shift is less pronounced than the shift of the peak in Re $k$. In the case shown in Fig. 2, the peak height and location are both apparently monotonic in $\delta_v$ near $\delta_v=1$; the peak shifts upward and to the right as $\delta_v$ decreases. This is not universal, however. In some cases (see, for example, Figs. 3 and 5, below), the peak height has its minimum when $\delta_v=1$, so that faster flow of *either* species raises the height of the instability peak. In one case we examined using the marginally stable $\alpha$-model with $\alpha=1$, the peak shifts to the right both for $\delta_v>1$ and $\delta_v<1$. What has been referred to as the differential flow instability can be understood as a special case in which a growth rate peak whose maximum is less than zero in the absence of differential flow is shifted above zero when $\delta_v\neq 1$, thus creating a convective instability even though the fixed point of the local system is stable. An example of this is shown in Fig. 3. Physically, the shifting of the peak relative to the phase velocity pole means that in the presence of differential flow the fastest-growing mode is a traveling wave with some finite velocity, rather than a uniform oscillation. From Fig. 2 it is evident that, while the amplitude ratio $R$ of the two species remains constant in the pure FDO case $\delta_v=1$, differential flow modifies both their amplitude and phase relations in a frequency-dependent manner.

Figure 4 shows the effect of differential diffusion without differential flow ($\delta_D\neq 1, \delta_v=1$). A family of solution curves is shown for $\delta_D\leqslant 1$ (i.e., equal diffusion or fast inhibitor diffusion). This is the case that renders a Turing instability possible in a stationary medium. The growth rate peak is distorted somewhat relative to that of the pure FDO case. This effect was more pronounced in some other examples we studied. In one case, fast inhibitor diffusion lowered and

broadened the FDO peak slightly while fast activator diffusion raised and sharpened the peak significantly. In any case, however, the distortion of the FDO peak is rather less salient than the growth of a second peak at a different frequency. When this second peak rises above zero, the modes contained within it have two important features: First, their phase velocity is close to 1. The phase velocity curves in Fig. 4 flatten out at $c \approx 1$ for the range of amplified frequencies in the second peak. This means that, in the comoving frame, the waves are stationary. Second, for frequencies within the range of the second peak, the imaginary part of the amplitude ratio Im $R$ is very small, indicating a lack of phase lag between the two components. Both of these observations are consistent with the Turing instability caused by differential diffusion. Because diffusion is directionally symmetric, a mechanism driven by differential diffusion cannot cause a phase lag between the two components. Turing patterns are reflection symmetric, and stationary in the comoving frame. In view of these observations we attribute the second peak to Turing-like modes and refer to it as a Turing peak. In this example it is quite clearly separated from the FDO peak, the latter being characterized by strongly frequency-dependent phase velocities and a nonzero imaginary component Im $R$ of the amplitude ratio. There is a range of frequencies between the two peaks for which there are only damped modes. In some cases, however, the two peaks can grow broader and almost merge, so that as the driving frequency changes, the resulting waves change continuously from a FDO-like to a Turing-like character. Even in such cases, the Turing modes are distinguishable by means of their near-unity phase velocities and nearly real amplitude ratios. The Turing modes correspond precisely to the wavelengths of Turing unstable modes in the stationary reaction-diffusion system, and the range of frequencies is therefore related to this wavelength range through the flow velocity. The range of FDO-unstable frequencies, by comparison, is approximately that given in Ref. [14] for the pure FDO case.

In Fig. 5, we examine the interaction between differential flow and differential diffusion, allowing both differential transport modes to operate simultaneously, as in Refs. [11–13]. Here we plot the dispersion solutions for a constant value of $\delta_D$ as $\delta_v$ varies. $\delta_D$ is such that a well-defined Turing peak exists for $\delta_v = 1$. We observe that setting $\delta_v \neq 1$ shifts the FDO peak as we expect. In this case, unlike that of Fig. 2 but similar to Fig. 3, the FDO peak grows higher for either fast activator or fast inhibitor flow. In contrast, the Turing peak is lowered for any $\delta_v \neq 1$. The two peaks appear to have a seesaw relation. Differential flow has other effects on the modes within the Turing peak. Their velocity begins to depart from unity and is less uniform across the peak, and the amplitude ratio is no longer purely real. In these senses, the "Turing" modes begin to lose their Turing-like character in the presence of differential flow, even though one can still perceive two separate peaks in the growth rate.

## III. NONLINEAR SIMULATIONS

We now show the results of some nonlinear simulations of the FitzHugh-Nagumo flow system in order to illustrate the application of the dispersion relations to experiments. We choose to simulate the FN model with $\varepsilon = 1.5$, $D = 0.05$, $\delta_v = 1$ and $\delta_D = 0.2$. As in the examples of Fig. 4, the dispersion relation shows both a FDO and a Turing peak. The natural oscillation frequency (the pole in the phase velocity) is $\omega_0 \approx 1.2$. For comparison with the simulations, we plot both solutions $k_\pm$ on the same axes, for physical frequencies $\omega > 0$. These plots are shown in Fig. 6. Figure 7 shows a series of simulations with different driving frequencies. The boundary conditions for these simulations were given by

$$\mathbf{u}(0,t) = a_0 \begin{pmatrix} \cos \omega t \\ \sin \omega t \end{pmatrix}$$

where $a_0 = 0.05$. The plots in the left column of this figure show the space-time patterns of the waves generated by the boundary perturbation. The dotted white line in each plot represents the trajectory of a point comoving with the flow. This allows the phase velocities of the waves to be compared readily with the flow velocity. The plots in the right column show both dynamical variables $a$ and $b$ as functions of posi-

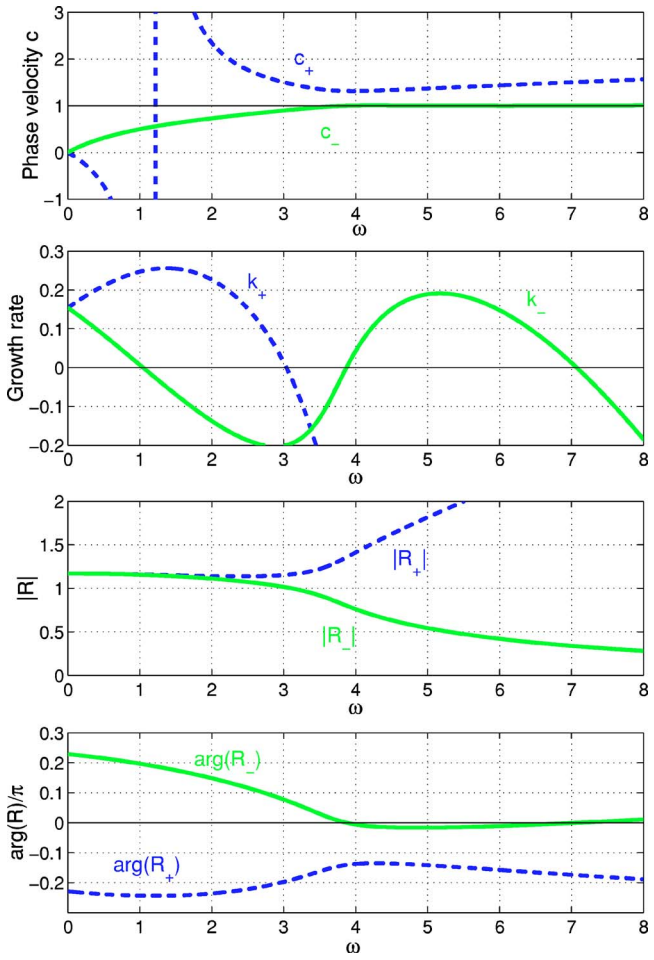


FIG. 6. (Color online) Growth rate, phase velocity, and modulus and phase of the complex amplitude ratio as functions of frequency for the model of our nonlinear simulations. Both relevant solutions are plotted. The modulus $|R|$ gives the ratio of the peak amplitudes for the oscillations of the two dynamical variables, while the phase or argument of $R$ gives the relative phase shift.

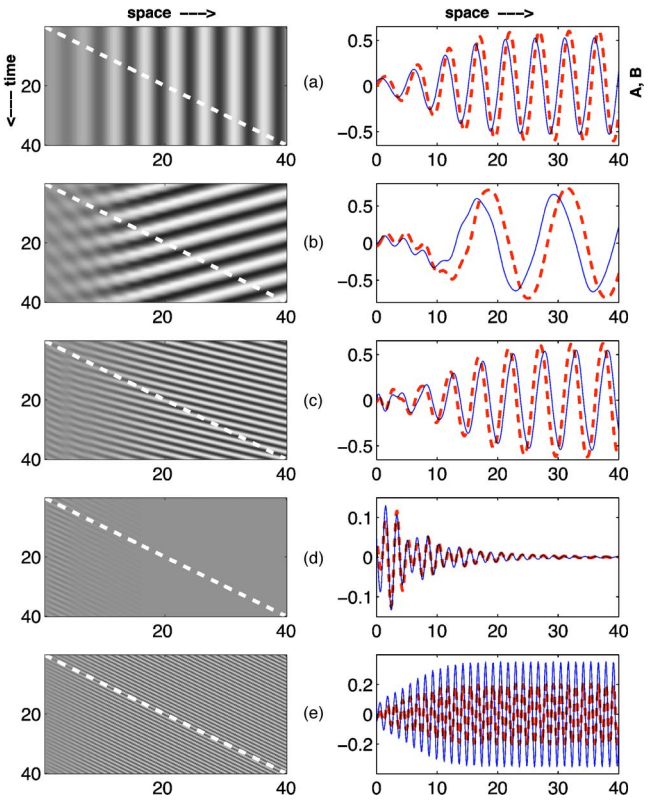


FIG. 7. (Color online) Results of nonlinear simulations of the FN model for sinusoidal boundary perturbations at five different frequencies (a) 0, (b) 0.9, (c) 2.5, (d) 3.5, and (e) 5. Left column: space (horizontal) vs time (vertical) plots with gray scale showing concentration $A$. Dotted white lines show the flow velocity. Right column: concentrations $A$ (thin line) and $B$ (thick dashed line) vs space (horizontal axis).

tion for a single time. The latter plots allow an examination of the wave forms, including the phase shifts between activator and inhibitor. The dispersion relation (Fig. 6) predicts a positive growth rate at $\omega=0$, and, accordingly, a constant (zero-frequency) perturbation indeed gives rise to growing stationary waves which saturate at a finite amplitude [Fig. 7(a)]. At $\omega=0.9$, below the natural frequency $\omega_0=1.2$, the dispersion relation shows that both $k_+$ and $k_-$ have positive growth rates, which are expected to compete. $k_-$ (the solid curve in Fig. 6) contributes waves with a phase velocity of $\sim 0.5$, i.e., downstream waves moving slower than the flow velocity, while $k_+$ gives waves with a negative phase velocity, i.e., upstream traveling waves. Near the boundary, a superposition of both waves occurs, but the upstream waves have a much larger growth rate and they dominate at positions farther downstream, crowding out the other mode entirely and reaching a nonlinear saturated amplitude [Fig. 7(b)]. At $\omega=2.5>\omega_0$, only $k_+$ has a positive growth rate, giving waves with a positive (downstream) phase velocity faster than the flow speed. A small admixture of the other mode $k_-$ can be discerned near the boundary, but it decays rapidly with downstream distance [Fig. 7(c)]. The asymptotic waves shown in Figs. 7(a)–7(c) agree qualitatively with the kinematic results.[2] $\omega=3.5$ falls within the gap between the FDO and Turing peaks. Thus there are no growing modes at this frequency and the disturbance decreases with downstream distance [Fig. 7(d)]. $\omega=5$, however, lies within the Turing peak of the $k_-$ solution. As predicted by the dispersion relation, the resulting waves have a velocity nearly equal to the flow velocity and there is almost no phase difference between the two species.

The amplitude and phase characteristics of the nonlinear wave forms (right column of Fig. 7) may also be compared with the predictions of the linear dispersion relation, and in this case the agreement is quite close. In the complex exponential solution Eq. (3), the modulus of the ratio $R=v/u$ gives the ratio of the peak amplitudes of the oscillations of the two dynamical variables, while the argument of $R$ gives the relative phase. For frequencies within the FDO peak, our nonlinear simulations show that, as one expects from Fig. 6, the ratio of the peak amplitudes of $b$ and $a$ is slightly larger than unity, while the phase shift is approximately $\pi/4 \approx \arg(R)$. For the Turing mode at $\omega=5$, on the other hand, the linear dispersion relation gives a very small phase shift for the relevant $k_-$ solution, and an amplitude ratio slightly larger than 0.5. The phase shift is indeed almost zero and the $b$ amplitude is indeed smaller than that of $a$. The actual amplitude ratio in the saturated waveform is approximately 0.6, close to the prediction of the linearized analysis.

Finally, we note that at frequencies where more than one mode is present, one can be selected by manipulating the driving function itself so as to align it with one eigenvector or the other. As an example, consider $\omega=0.9$, a frequency at which both solution branches exhibit positive growth rates. Here, we find that for the faster-growing $k_+$ mode the complex amplitude ratio is $R_+ \approx 0.84-0.8i$ while for the other mode $R_- \approx 0.94+0.68i$. The driving function used in Fig. 7 excites both of these modes and a superposition is seen near the upstream boundary. By tuning the driving function to be

$$\mathbf{u}(0,t) = a_0 \,\mathrm{Re}\begin{pmatrix} 1 \\ R_+ \end{pmatrix} e^{i\omega t} = a_0 \,\mathrm{Re}\begin{pmatrix} e^{i\omega t} \\ |R_+| e^{i(\omega t+\phi_+)} \end{pmatrix}$$

$$= a_0 \begin{pmatrix} \cos \omega t \\ 0.84 \cos \omega t + 0.8 \sin \omega t \end{pmatrix},$$

however, we can excite mostly the $k_+$ mode so that the upstream traveling waves appear almost uncontaminated. Conversely, by choosing the amplitude and phase of the driving to align with the other eigenvector, we excite mostly the other, $k_-$ mode. Eventually, however, the faster-growing $k_+$ mode begins to appear, possibly through nonlinear effects or

[2]The kinematics of FDO waves is governed by the readily calculable [7,8,19] phase function $\phi(t,x)$ of the medium that oscillates with natural frequency $\omega_0$, is periodically forced at the inflow at frequency $\omega$, and flows with velocity $v$. The phase velocity follows as $c=v/(1-\omega_0/\omega)$ and the wavelength as $\lambda=|v/\omega|$. Note the stationary wave $c=0$ at $\omega=0$, the pole $c=\infty$ at $\omega/\omega_0=1$, and the reversal of the phase velocity from upstream propagating $c<0$ for $\omega_0/\omega>1$ to downstream propagating $c>0$ for $\omega_0/\omega<1$, all in agreement with experiments [7,19].

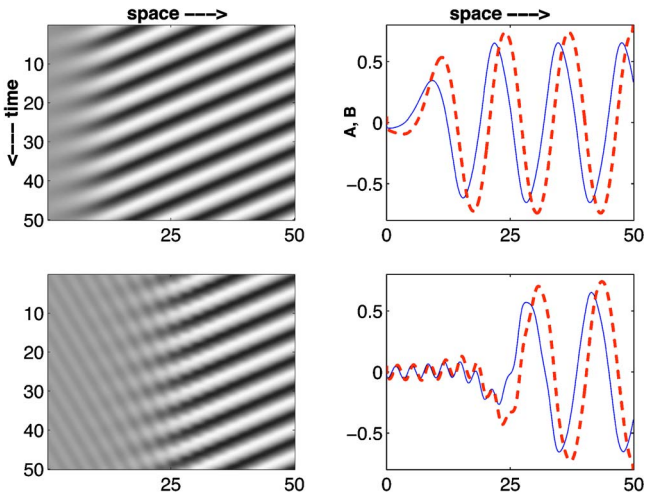


FIG. 8. (Color online) Simulations with sinusoidal boundary perturbations at $\omega=0.9$, but with the driving amplitudes and phases tuned to select the upstream (top) or downstream (bottom) mode. Even if the downstream mode is selected near the boundary, the faster-growing upstream mode eventually takes over farther downstream. As in Fig. 7, the plots on the left are space-time, and those on the right are of $A$ and $B$ vs position.

through the small admixture still present in the boundary condition, and the $k_+$ mode eventually wins in the asymptotic downstream region. Simulation results which show this selection effect are plotted in Fig. 8.

## IV. CONCLUSIONS AND EXPERIMENTAL TESTS

We have examined the linear stability analysis relevant to the convective growth of spatiotemporal patterns in a reactive flow system, excited by a small sinusoidal perturbation of a fixed point at the inflow boundary. We examined the real and imaginary parts of the wave number as functions of the real boundary forcing frequency. They represent the downstream growth rate and periodicity of the disturbances caused by a boundary perturbation. We found that the growth rate as a function of frequency exhibits at most two physically distinct peaks corresponding to two types of waves, one or both of which may be present and convectively unstable. We found that, in addition to the phase velocity, the complex ratio $R$ of activator and inhibitor concentrations, which encodes the relative amplitude and phase of oscillations in the activator and inhibitor concentrations, provides an additional criterion for distinguishing the types of modes. Turing-like modes are distinguished from FDO-like modes by the lack of a phase lag between the two components and by phase velocities that are close to the flow velocity, so that in the comoving frame they are stationary patterns. Viewing the different types of modes as belonging to peaks in the growth rate, we saw the close relationship between FDO and the differential flow instability. One can be viewed as a continuous deformation of the other. A primary effect of differential flow is to shift the FDO peak. What has been referred to as the differential flow instability (the appearance of a traveling wave instability in a medium which is neither Hopf nor Turing unstable) can be interpreted as a case in which a subthreshold FDO peak is shifted sufficiently to bring it above zero and to create unstable modes (Fig. 3).

We now comment on experimental verifications of the present predictions. The presence of two peaks could be seen in an experiment in which the perturbation frequency at the inflow is the control parameter. Frequencies for which the growth rate is positive will result in sustained waves, while the waves will die out and fail to propagate if the growth rate is negative. Based on our results we expect that growing waves will appear within at most two frequency ranges. The phase velocities can also be measured and compared with our general findings.

Two types of experiments may be envisaged, in which oscillatory driving is implemented differently. The first type [20,32,22] makes use of a linearly growing, light-sensitive reaction-diffusion system. The effective moving boundary is provided by a moving mask which extinguishes the reaction on the illuminated side of a moving line. The illumination at the moving boundary can be modulated periodically, resulting in an oscillatory perturbation. In these experiments, differential diffusion $\delta_D \neq 1$ is achieved by immobilizing one species on a gel, but differential flow is absent, $\delta_v=1$.

The second type of experiment is conducted in a packed bed reactor, which is fed by the outlet of a continuous stirred tank reactor [5,16–19,21]. The CSTR may be manipulated to be stationary or to oscillate slower or faster than the medium in the PBR. This leads to stationary and upstream and downstream moving waves, respectively [5–7,19,8]. By packing the PBR with ion-exchanger beads that immobilize either activator or inhibitor, conditions of simultaneous differential diffusion and differential flow may be obtained. References [11,12] modeled this by setting $\delta_D=\delta_v$.

It is a challenge to devise experiments in which the flow ratio, diffusion ratio, and driving frequency can be varied independently. While the phase velocities of traveling waves can easily be measured, verification of other properties of the waves may present experimental challenges. Verification of the predicted phase relationships would require simultaneous measurements of both activator and inhibitor concentrations.

[1] P. Andresen, M. Bache, E. Mosekilde, G. Dewel, and P. Borckmanns, Phys. Rev. E **60**, 297 (1999).
[2] S. P. Kuznetsov, E. Mosekilde, G. Dewel, and P. Borckmanns, J. Chem. Phys. **106**, 7609 (1997).
[3] J. R. Bamforth, S. Kalliadasis, J. H. Merkin, and S. K. Scott, Phys. Chem. Chem. Phys. **2**, 4013 (2000).
[4] J. R. Bamforth, J. H. Merkin, S. K. Scott, R. Toth, and V. Gaspar, Phys. Chem. Chem. Phys. **3**, 1435 (2001).
[5] M. Kaern and M. Menzinger, Phys. Rev. E **60**, R3471 (1999); **62**, 2994 (2000); P. Andresen, E. Mosekilde, G. Dewel, and P.

Borckmans, *ibid.* **62**, 2992 (2000).
[6] M. Kaern, M. Menzinger, and A. Hunding, Biophys. Chem. **87**, 121 (2000).
[7] M. Kaern, M. Menzinger, and A. Hunding, J. Theor. Biol. **207**, 473 (2000).
[8] M. Kaern, M. Menzinger, R. Satnoianu, and A. Hunding, Faraday Discuss. **120**, 295 (2002).
[9] A. B. Rovinsky and M. Menzinger, Phys. Rev. Lett. **69**, 1193 (1992).
[10] X. G. Wu, S. Nakata, M. Menzinger, and A. Rovinsky, J. Phys. Chem. **100**, 15810 (1996).
[11] R. A. Satnoianu and M. Menzinger, Phys. Rev. E **62**, 113 (2000).
[12] R. Satnoianu, P. K. Maini, and M. Menzinger, Physica D **160**, 79 (2001).
[13] R. A. Satnoianu, Phys. Rev. E **68**, 032101 (2003).
[14] P. McGraw and M. Menzinger, Phys. Rev. E **68**, 066122 (2003).
[15] D. Vasquez, Phys. Rev. Lett. **93**, 104501 (2004).
[16] J. R. Bamforth, R. Toth, V. Gaspar, and S. K. Scott, Phys. Chem. Chem. Phys. **4**, 1299 (2002).
[17] R. Toth, A. Papp, V. Gaspar, J. H. Merkin, S. K. Scott, and A. F. Taylor, Phys. Chem. Chem. Phys. **3**, 957 (2001).
[18] M. Kaern and M. Menzinger, Phys. Rev. E **61**, 3334 (2000).
[19] M. Kaern and M. Menzinger, J. Phys. Chem. A **106**, 4897 (2002).
[20] M. Kaern, D. G. Miguez, A. P. Munuzuri, and M. Menzinger, Biophys. Chem. **110**, 231 (2004).
[21] A. B. Rovinsky and M. Menzinger, Phys. Rev. Lett. **70**, 778 (1993).
[22] M. Kaern, R. Satnoianu, A. Munuzuri, and M. Menzinger, Phys. Chem. Chem. Phys. **4**, 1315 (2002).
[23] A. M. Turing, Philos. Trans. R. Soc. London, Ser. B **237**, 37 (1952).
[24] R. Kapral and K. Showalter, *Chemical Waves and Patterns* (Kluwer, Dorderecht, 1995).
[25] M. Menzinger and A. B. Rovinsky, *Chemical Waves and Patterns*, edited by R. Kapral and K. Showalter (Kluwer, Dordrecht, 1995).
[26] R. J. Briggs, *Electron-Stream Interaction with Plasmas* (MIT Press, Cambridge, MA, 1964), pp. 8–46.
[27] M. R. E. Proctor, S. M. Tobias, and E. Knobloch, Physica D **145**, 191 (2000).
[28] R. J. Deissler, J. Stat. Phys. **40**, 371 (1985); **54**, 1459 (1989).
[29] L. Wolpert, *Principles of Development* (Oxford University Press, Oxford, 1998).
[30] J. D. Murray, *Mathematical Biology II: Spatial Models and Biomedical Applications* (Springer, Berlin, 2003).
[31] C. B. Muratov and V. V. Osipov, Phys. Rev. E **54**, 4860 (1996); S. P. Dawson, M. V. D'Angelo, and J. E. Pearson, Phys. Lett. A **265**, 346 (2000); A. Hagberg and E. Meron, Chaos **4**, 477 (1994).
[32] D. G. Miguez, R. Satnoianu, and A. P. Munuzuri (unpublished).